A FINITE DIFFERENCE TECHNIQUE FOR SIMULATING THREE-DIMENSIONAL NON-NEWTONIAN FREE SURFACE FLOWS

M. F. Tomé – murilo@lcad.icmc.sc.usp.br
N. Mangiavacchi – norberto@lcad.icmc.sc.usp.br
A. Castelo – castelo@icmc.sc.usp.br
J. A. Cuminato – jacumina@lcad.icmc.sc.usp.br
A. Fortuna – fortuna@lcad.icmc.sc.usp.br
L. G. Nonato – nonato@lcad.icmc.sc.usp.br
L. Grossi – luciane@lcad.icmc.sc.usp.br
V. G. Ferreira – pvgf@lcad.icmc.sc.usp.br
Universidade de São Paulo, Departamento de Ciências de Computação e Estatística
Cx.P. 668 – 13560-161 – São Carlos, SP, Brasil
Sean McKee – caas29@maths.strath.ac.uk
University of Strathclyde, Department of Mathematics
Glasgow, Scotland

Abstract. *This work presents a numerical technique for solving three-dimensional non-Newtonian free surface flows. It is an extension of the technique introduced by Tomé, McKee and Duffy (1996) to three dimensions. The governing equations are solved by the finite difference method on a staggered grid. It uses marker particles to describe the fluid which provides the location and visualization of the free surface. As currently implemented, the present method can simulate the flow of Cross and Power-law modelled fluids. Results demonstrating the capability of this technique for solving industrial problems are presented. In particular, results which simulate the flow of a non-Newtonian fluid jet impinging onto a flat surface are given.*

Keywords: *Free surface flows, Cross model, finite difference, non-Newtonian fluid*

1. INTRODUCTION

Non-Newtonian fluid flows with free surfaces appear in many technological processes: container filling (food industry), injection moulding (plastic industries), ink jet devices, wire coating, among others, are all examples of non-Newtonian free surface flows problems. Many numerical techniques have been proposed over the past three decades to treat non-Newtonian flows. Today there is an intense activity in this area: a general overview of free surface flows can be found in the books of Shyy *et al.* (1996) and Griebel *et al.* (1997) (see also Mompean, 1997; Brasseur *et al.*, 1998; Ding *et al.*, 1993). This paper describes a numerical technique for solving three-dimensional non-Newtonian free surfaces flows. The governing equations of

a generalized fluid are considered and a solution procedure is presented. As a test problem we simulated the flow of a non-Newtonian jet impinging onto a flat surface. The numerical results obtained with the Cross model agree qualitatively with the theory.

2. GOVERNING EQUATIONS

The basic equations for the flow of an incompressible generalized fluid with density ρ can be written as

$$\rho\frac{D\mathbf{u}}{Dt} = \nabla\cdot\underline{\underline{\boldsymbol{\sigma}}} + \rho\mathbf{g}\,, \quad \nabla\cdot\mathbf{u} = 0 \tag{1}$$

where $\mathbf{u}(\mathbf{x},t)$, $\sigma(\mathbf{x},t)$ and $\mathbf{g}$ denote the fluid velocity, the stress tensor and gravitational acceleration, respectively. The stress tensor is required to obey the constitutive equations

$$\underline{\underline{\boldsymbol{\sigma}}} = -p\,\underline{\underline{\mathbf{I}}} + 2\nu(q)\,\underline{\underline{\mathbf{d}}} \tag{2}$$

where p is the fluid pressure, $\underline{\underline{\mathbf{I}}}$ is the identity tensor, $\underline{\underline{\mathbf{d}}}$ is the rate-of-deformation tensor

$$\underline{\underline{\mathbf{d}}} = \frac{1}{2}\left[(\nabla\mathbf{u}) + (\nabla\mathbf{u})^T\right]\,, \tag{3}$$

q is the local shear rate defined by

$$q = \left[2\mathrm{tr}(\underline{\underline{\mathbf{d}}}^2)\right]^{1/2} \tag{4}$$

and $\mu(q)$ is the apparent viscosity (a prescribed function of q). Introducing Eq. (2) and Eq. (3) into Eq. (1) we obtain

$$\frac{D\mathbf{u}}{Dt} = -\nabla p + \nu(q)\nabla^2\mathbf{u} + \nabla\nu(q)\left[(\nabla\mathbf{u}) + (\nabla\mathbf{u})^{\mathrm{T}}\right] + \mathbf{g}, \tag{5}$$

$$\nabla\cdot\mathbf{u} = 0, \tag{6}$$

where $\nu(q)$ is the kinematic viscosity. We shall consider unsteady free-surface flows of viscous fluid moving into a passive atmosphere (which we may take to be at zero pressure). In the absence of surface tension the normal and tangential components of stress must be continuous across any free surface, so that on such a surface

$$\mathbf{n}\cdot(\underline{\underline{\boldsymbol{\sigma}}}\cdot\mathbf{n}) = 0 \quad \text{and} \quad \mathbf{m}\cdot(\underline{\underline{\boldsymbol{\sigma}}}\cdot\mathbf{n}) = 0, \tag{7}$$

where $\mathbf{n}$ and $\mathbf{m}$ denote unit normal and tangent vectors to the surface and $\underline{\underline{\boldsymbol{\sigma}}}$ denotes the stress tensor. We also have the no-slip condition ($\mathbf{u} = \mathbf{0}$) on fixed boundaries. Other boundary conditions, such as those at an entry or exit port to the computational domain, are discussed in Tomé, Duffy and McKee (1996). We consider three-dimensional flows and use Cartesian coordinates, with
$\mathbf{u} = (u(x,y,z,t), v(x,y,z,t), w(x,y,z,t))$ and $p = p(x,y,z,t)$. With L, U and ν_0 denoting 'typical' length, velocity and viscosity scales, we introduce the nondimensionalization

$$\mathbf{u} = U\bar{\mathbf{u}}, \quad \mathbf{x} = L\bar{\mathbf{x}}, \quad \nu = \nu_0\bar{\nu}, \quad q = \frac{U}{L}\bar{q}, \quad t = \frac{L}{U}\bar{t}, \quad p = \rho U^2\bar{p}, \quad \mathbf{g} = g\bar{\mathbf{g}},$$

where $g = |\mathbf{g}|$ (so that $\bar{\mathbf{g}}$ is a unit vector). For the sake of clarity we drop the overbars so that Eq. (5) and Eq. (6) may be written as

$$\frac{\partial \mathbf{u}}{\partial t} = -\nabla p + N(\mathbf{u}) \tag{8}$$

$$\frac{\partial u}{\partial x} + \frac{\partial v}{\partial y} + \frac{\partial w}{\partial z} = 0 \tag{9}$$

where $N(\mathbf{u})$ has components

$$\begin{aligned} N_1 &= -\frac{\partial u^2}{\partial x} - \frac{\partial (uv)}{\partial y} - \frac{\partial (uw)}{\partial z} + \frac{1}{\mathrm{Re}}\nu(q)\left[\frac{\partial^2 u}{\partial x^2} + \frac{\partial^2 u}{\partial y^2} + \frac{\partial^2 u}{\partial z^2}\right] \\ &\quad + \frac{1}{\mathrm{Re}}\left[2\frac{\partial u}{\partial x}\frac{\partial \nu}{\partial x} + \left(\frac{\partial u}{\partial y} + \frac{\partial v}{\partial x}\right)\frac{\partial \nu}{\partial y} + \left(\frac{\partial u}{\partial z} + \frac{\partial w}{\partial x}\right)\frac{\partial \nu}{\partial z}\right] + (1/\mathrm{Fr}^2)g_x \end{aligned} \tag{10}$$

$$\begin{aligned} N_2 &= -\frac{\partial (uv)}{\partial x} - \frac{\partial (v^2)}{\partial y} - \frac{\partial (vw)}{\partial z} + \frac{1}{\mathrm{Re}}\nu(q)\left[\frac{\partial^2 v}{\partial x^2} + \frac{\partial^2 v}{\partial y^2} + \frac{\partial^2 v}{\partial z^2}\right] \\ &\quad + \frac{1}{\mathrm{Re}}\left[\left(\frac{\partial u}{\partial y} + \frac{\partial v}{\partial x}\right)\frac{\partial \nu}{\partial x} + 2\frac{\partial v}{\partial y}\frac{\partial \nu}{\partial y} + \left(\frac{\partial v}{\partial z} + \frac{\partial w}{\partial y}\right)\frac{\partial \nu}{\partial z}\right] + (1/\mathrm{Fr}^2)g_y \end{aligned} \tag{11}$$

$$\begin{aligned} N_3 &= -\frac{\partial (uw)}{\partial x} - \frac{\partial (vw)}{\partial y} - \frac{\partial (w^2)}{\partial z} + \frac{1}{\mathrm{Re}}\nu(q)\left[\frac{\partial^2 w}{\partial x^2} + \frac{\partial^2 w}{\partial y^2} + \frac{\partial^2 w}{\partial z^2}\right] \\ &\quad + \frac{1}{\mathrm{Re}}\left[\left(\frac{\partial u}{\partial z} + \frac{\partial w}{\partial x}\right)\frac{\partial \nu}{\partial x} + \left(\frac{\partial v}{\partial z} + \frac{\partial w}{\partial y}\right)\frac{\partial \nu}{\partial y} + 2\frac{\partial w}{\partial z}\frac{\partial \nu}{\partial z}\right] + (1/\mathrm{Fr}^2)g_z \end{aligned} \tag{12}$$

where $\mathrm{Re} = UL/\nu$ and $\mathrm{Fr} = U/\sqrt{Lg}$ are the associated Reynolds number and Froude number respectively. The local shear rate Eq. (4) is given by

$$q = \left[2\left(\frac{\partial u}{\partial x}\right)^2 + 2\left(\frac{\partial v}{\partial y}\right)^2 + 2\left(\frac{\partial w}{\partial z}\right)^2 + \left(\frac{\partial u}{\partial y} + \frac{\partial v}{\partial x}\right) + \left(\frac{\partial u}{\partial z} + \frac{\partial w}{\partial x}\right) + \left(\frac{\partial v}{\partial z} + \frac{\partial w}{\partial y}\right)\right]^{1/2}. \tag{13}$$

The viscosity $\nu(q)$ can be any function of q representing the shear-thinning nature of the fluid. In the simulations, we employ the Cross Model,

$$\frac{\nu - \nu_\infty}{\nu_0 - \nu_\infty} = \frac{1}{(1 + (Kq)^m)}, \qquad \text{where } m, \nu_0, \nu_\infty \text{ and K are given positive constants.} \tag{14}$$

3. PROCEDURE

To solve Eq. (8) and Eq. (9) we employ the following procedure which is the 3D-version of GENSMAC (see Tomé, Duffy and McKee, 1996).
Let us suppose that at a given time, say t_0, the velocity field $\mathbf{u}(\mathbf{x}, t_0)$ is known and boundary conditions for the velocity and pressure are given. To compute the velocity field and the pressure field at the advanced time $t = t_0 + \delta t$, we proceed as follows:

Step 1: Compute $q(x, y, z, t_0)$ and $\nu(x, y, z, t_0)$ using $\mathbf{u}(x, y, z, t_0)$

Step 2: Let $\tilde{p}(x, y, z, t)$ be a pressure field which satisfies the correct pressure condition on the free surface.

Step 2: Calculate the intermediate velocity field, $\tilde{\mathbf{u}}(x, y, z, t)$, from

$$\frac{\partial \tilde{\mathbf{u}}}{\partial t} = -\nabla \tilde{p} + N(\mathbf{u}) \tag{15}$$

with $\tilde{\mathbf{u}}(x, y, z, t_0) = \mathbf{u}(x, y, z, t_0)$ using the correct boundary conditions for $\mathbf{u}(x, y, z, t_0)$. The components of $N(\mathbf{u})$ are definided by Eqs. (10)–(12). These equations are solved by the finite difference method.

Step 3: Solve the Poisson equation

$$\nabla^2 \psi(x, y, z, t) = \nabla . \tilde{\mathbf{u}}(x, y, z, t). \tag{16}$$

The appropriate boundary conditions for this equation are (see Tomé & McKee, 1994)

$$\frac{\partial \psi}{\partial n} = 0 \qquad \text{on rigid boundaries and} \qquad \psi = 0 \qquad \text{on the free surface.}$$

Step 4: Compute the velocity field

$$\mathbf{u}(x, y, z, t) = \tilde{\mathbf{u}}(x, y, z, t) - \nabla \psi(x, y, z, t). \tag{17}$$

Step 5: Compute the pressure

$$p(x, y, z, t) = \tilde{p}(x, y, z, t_0) + \frac{\psi(x, y, z, t)}{\delta t}. \tag{18}$$

Thus, we solve the momentum equations explicitly followed by a sparse symmetric system (the discrete Poisson equation) for the potential function ψ. For container filling problems the order of this system is continually increasing (since one only solves for $\mathbf{u}$ and p within the bulk fluid).

3.1 Boundary conditions

The rigid boundary conditions currently implemented are of no-slip and prescribed inflow types. They are applied on the rigid boundaries (containers and inflow boundaries) in contact with the fluid and require the calculation of the intersections of lines parallel to the sides of the cells with the containers. These intersections are calculated only once and stored in a tree structure representing the cells in the structures Container and Inflow. For details see Castelo *et. al.* (2000).

4. BASIC FINITE DIFFERENCE EQUATIONS

For solving **Steps 1** to **5** of the procedure presented in the previous Section we employ the following approach. A staggered grid is used. A typical cell is shown in Fig. 1. The variables $p_{i,j,k}$, the potential function $\psi_{i,j,k}$ and the discrete shear rate $q_{i,j,k}$ are positioned at a cell centre while $u_{i,j,k}$, $v_{i,j,k}$ and $w_{i,j,k}$ are staggered by a translation of $\delta x/2$, $\delta y/2$ and $\delta z/2$ respectively. A scheme for identifying the free surface and the fluid region is employed. To accomodate this, the cells within the mesh are defined as full cells (F), surface cells (S), empty cells (E) and boundary cells (B). A detailed description of these is given in Tomé *et. al.* (2000). The momentum equation Eq. (15) is discretized and applied at $u-$nodes, $v-$nodes and $w-$nodes respectively. The time derivative is discretized explicitly while the Laplacian is approximated by central differences. The convective terms are first averaged and then are discretized using central differences. Details of these approximations are given in Tomé *et. al.* (2000). Therefore, Eq. (15) is approximated by the following difference equations

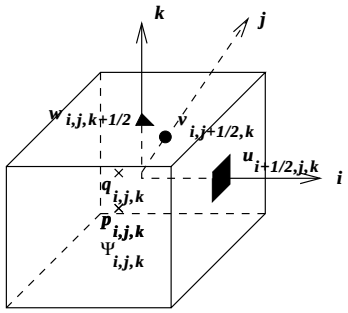

Figure 1. Typical cell used in a calculational time-step.

$$\tilde{u}_{i+\frac{1}{2},j,k} = u_{i+\frac{1}{2},j,k} - \delta t \left[u_{i+\frac{1}{2},j,k} \left(\frac{u_{i+\frac{3}{2},j,k} - u_{i-\frac{1}{2},j,k}}{\delta x} \right) + \frac{\tilde{p}_{i+1,j,k} - \tilde{p}_{i,j,k}}{\delta x} \right.$$
$$+ \frac{1}{4\delta y} \left((u_{i+\frac{1}{2},j,k} + u_{i+\frac{1}{2},j+1,k})(v_{i,j+\frac{1}{2},k} + v_{i+1,j+\frac{1}{2},k}) - (u_{i+\frac{1}{2},j,k} + u_{i+\frac{1}{2},j-1,k}) \right.$$
$$\left. (v_{i,j-\frac{1}{2},k} + v_{i+1,j-\frac{1}{2},k}) \right) + \frac{1}{4\delta z} \left((u_{i+\frac{1}{2},j,k} + u_{i+\frac{1}{2},j,k+1})(w_{i,j,k+\frac{1}{2}} + w_{i+1,j,k+\frac{1}{2}}) \right.$$
$$\left. - (u_{i+\frac{1}{2},j,k} + u_{i+\frac{1}{2},j,k-1})(w_{i,j,k-\frac{1}{2}} + w_{i+1,j,k-\frac{1}{2}}) \right) - \frac{1}{\mathrm{Re}} \nu(q_{i+\frac{1}{2},j,k}) \left(\frac{u_{i-\frac{1}{2},j,k} - 2u_{i+\frac{1}{2},j,k}}{\delta x^2} \right.$$
$$\left. + \frac{u_{i+\frac{3}{2},j,k}}{\delta x^2} + \frac{u_{i+\frac{1}{2},j-1,k} - 2u_{i+\frac{1}{2},j,k} + u_{i+\frac{1}{2},j+1,k}}{\delta y^2} + \frac{u_{i+\frac{1}{2},j,k-1} - 2u_{i+\frac{1}{2},j,k}}{\delta z^2} \right.$$
$$\left. + u_{i+\frac{1}{2},j,k+1} \right) - \frac{1}{\mathrm{Re}} \left(\left(\frac{u_{i+\frac{3}{2},j,k} - u_{i-\frac{1}{2},j,k}}{\delta x} \right) \frac{\partial \nu(q)}{\partial x}|_{i+\frac{1}{2},j,k} + \left(\frac{u_{i+\frac{1}{2},j+1,k} - u_{i+\frac{1}{2},j-1,k}}{2\delta y} \right.\right.$$
$$\left.\left. + \frac{v_{i+1,j+\frac{1}{2},k} + v_{i+1,j-\frac{1}{2},k} - v_{i,j+\frac{1}{2},k} - v_{i,j-\frac{1}{2},k}}{2\delta x} \right) \frac{\partial \nu(q)}{\partial y}|_{i+\frac{1}{2},j,k} + \left(\frac{u_{i+\frac{1}{2},j,k+1} - u_{i+\frac{1}{2},j,k-1}}{2\delta z} \right.\right.$$
$$\left.\left. + \frac{w_{i+1,j,k+\frac{1}{2}} + w_{i+1,j,k-\frac{1}{2}} - w_{i,j,k+\frac{1}{2}} - w_{i,j,k-\frac{1}{2}}}{2\delta x} \right) \frac{\partial \nu(q)}{\partial z}|_{i+\frac{1}{2},j,k} \right) - \frac{1}{\mathrm{Fr}^2} g_x \Bigg] \qquad (19)$$

and similar expressions for the v and w components. The Poisson equation Eq. (18) is discretized at cell centres using the seven-point Laplacian, namely,

$$\frac{\psi_{i+1,j,k} - 2\psi_{i,j,k} + \psi_{i-1,j,k}}{\delta x^2} + \frac{\psi_{i,j+1,k} - 2\psi_{i,j,k} + \psi_{i,j-1,k}}{\delta y^2} + \frac{\psi_{i,j,k+1} - 2\psi_{i,j,k} + \psi_{i,j,k-1}}{\delta z^2} = \tilde{D}_{i,j,k} \qquad (20)$$

where $\tilde{D}_{i,j,k} = \dfrac{\tilde{u}_{i+\frac{1}{2},j,k} - \tilde{u}_{i-\frac{1}{2},j,k}}{\delta x} + \dfrac{\tilde{v}_{i,j+\frac{1}{2},k} - \tilde{v}_{i,j-\frac{1}{2},k}}{\delta y} + \dfrac{\tilde{w}_{i,j,k+\frac{1}{2}} - \tilde{w}_{i,j,k-\frac{1}{2}}}{\delta z}$.

The velocity at the advanced time t_{n+1} is obtained by discretizing Eq. (17) at the respective nodes, namely,

$$\begin{cases} u_{i+\frac{1}{2},j,k} = \tilde{u}_{i+\frac{1}{2},j,k} - \left(\dfrac{\psi_{i+1,j,k} - \psi_{i,j,k}}{\delta x} \right), \\ v_{i,j+\frac{1}{2},k} = \tilde{v}_{i,j+\frac{1}{2},k} - \left(\dfrac{\psi_{i,j+1,k} - \psi_{i,j,k}}{\delta y} \right), \\ w_{i,j,k+\frac{1}{2}} = \tilde{w}_{i,j,k+\frac{1}{2}} - \left(\dfrac{\psi_{i,j,k+1} - \psi_{i,j,k}}{\delta z} \right). \end{cases} \qquad (21)$$

Equation (20) leads to a symmetric and positive definite linear system for $\psi_{i,j,k}$. In order to solve this linear system we employ the conjugate gradient method as implemented in GENSMAC (see Tomé & McKee, 1994). Therefore, a calculational cycle consists of solving Eqs. (19)–(21) for a given time-step.

4.1 Free surface stress conditions

Let $\mathbf{n}$, $\mathbf{m_1}$, and $\mathbf{m_2}$ denote unit normal and tangential vectors on the free surface. Then, conditions Eq. (7) can be written as

$$p - \frac{2}{\mathrm{Re}}\nu(q)\left[\frac{\partial u}{\partial x}n_x^2 \quad + \quad \frac{\partial v}{\partial y}n_y^2 + \frac{\partial w}{\partial z}n_z^2 + \left(\frac{\partial u}{\partial y} + \frac{\partial v}{\partial x}\right)n_x n_y + \left(\frac{\partial u}{\partial z} + \frac{\partial w}{\partial x}\right)n_x n_z + \left(\frac{\partial v}{\partial z} + \frac{\partial w}{\partial y}\right)n_y n_z\right] = 0\,, \tag{22}$$

$$\frac{1}{\mathrm{Re}}\left[2\frac{\partial u}{\partial x}m1_x n_x + 2\frac{\partial v}{\partial y}m1_y n_y + 2\frac{\partial w}{\partial z}m1_z n_z + \left(\frac{\partial u}{\partial y} + \frac{\partial v}{\partial x}\right)(m1_x n_y + m1_y n_x) + \left(\frac{\partial u}{\partial z} + \frac{\partial w}{\partial x}\right)(m1_x n_z + m1_z n_x) + \left(\frac{\partial v}{\partial z} + \frac{\partial w}{\partial y}\right)(m1_y n_z + m1_z n_y)\right] = 0\,, \tag{23}$$

$$\frac{1}{\mathrm{Re}}\left[2\frac{\partial u}{\partial x}m2_x n_x + 2\frac{\partial v}{\partial y}m2_y n_y + 2\frac{\partial w}{\partial z}m2_z n_z + \left(\frac{\partial u}{\partial y} + \frac{\partial v}{\partial x}\right)(m2_x n_y + m2_y n_x) + \left(\frac{\partial u}{\partial z} + \frac{\partial w}{\partial x}\right)(m2_x n_z + m2_z n_x) + \left(\frac{\partial v}{\partial z} + \frac{\partial w}{\partial y}\right)(m2_y n_z + m2_z n_y)\right] = 0\,, \tag{24}$$

respectively. In order to apply these conditions we employ the ideas presented by Tomé & McKee (1994) as follows. Let us suppose that the mesh spacing is small enough so that, locally, the free surface can be approximated by a planar surface. Then Eqs. (22)–(24) can be approximated by local finite differences according to three cases: planar surface parallel to a coordinate axis, 45^0-sloped planar surface and 45^0-sloped planar surface. Details of the corresponding finite difference equations involved for each case are given in Tomé *et. al.* (2000).

4.2 Time-step control and free surface movement

A procedure for calculating the time-step is employed. The time-step size is computed according to the following stability restrictions

$$\delta t < \frac{\delta x}{|u|}\,, \quad \delta t < \frac{\delta y}{|v|}\,, \quad \delta t < \frac{\delta z}{|w|}, \quad \delta t < \frac{\delta x^2\delta y^2\delta z^2}{\delta x^2\delta y^2 + \delta x^2\delta z^2 + \delta y^2\delta z^2}\frac{\mathrm{Re}}{2}\frac{1}{\nu_{max}}, \tag{25}$$

where ν_{max} is maximum value of the viscosity whithin the bulk fluid (normally taken as 1). The implementation of this time-step procedure follows the same ideas of Tomé, Duffy and McKee (1996). The fluid is represented by a B-Rep data structure (see Mäntylä, 1988). The fluid surface is defined by a piecewise linear surface composed of triangles and/or quadrilaterals containing marker particles on their vertices. The fluid surface is updated in three stages: firstly, the surface is moved to the new location according to the newly computed velocity field, in the second stage new particles are inserted if required and thirdly, particles are removed from cells which have accumulated too many. A fluid particle moves according to the equation

$$\frac{d\mathbf{x}_p}{dt} = \mathbf{u}_p\,,$$

where $\mathbf{u}_p$ is the velocity of the particle at time t_{n+1}. By using Euler's method, the particles are moved to the new position

$$x^{n+1} = x^n + u_p\delta t, \qquad y^{n+1} = y^n + v_p\delta t, \qquad z^{n+1} = z^n + w_p\delta t,$$

where x^n, y^n, z^n is the position of particle p. The particle velocities u_p, v_p, z_p are found by performing a tri-linear approximation using the eight nearest velocities.
Details of particle insertion and particle removal are given in Castelo *et. al. (2000).*

5. NUMERICAL RESULTS

The finite difference equations described in Section 4 were incorporated into the Freeflow–3D code in order to simulate unsteady non-Newtonian free surface flow. We present several calculations which demonstrate that the technique presented in this paper can indeed simulate flows of a shear thinning fluid. The results are as follows.

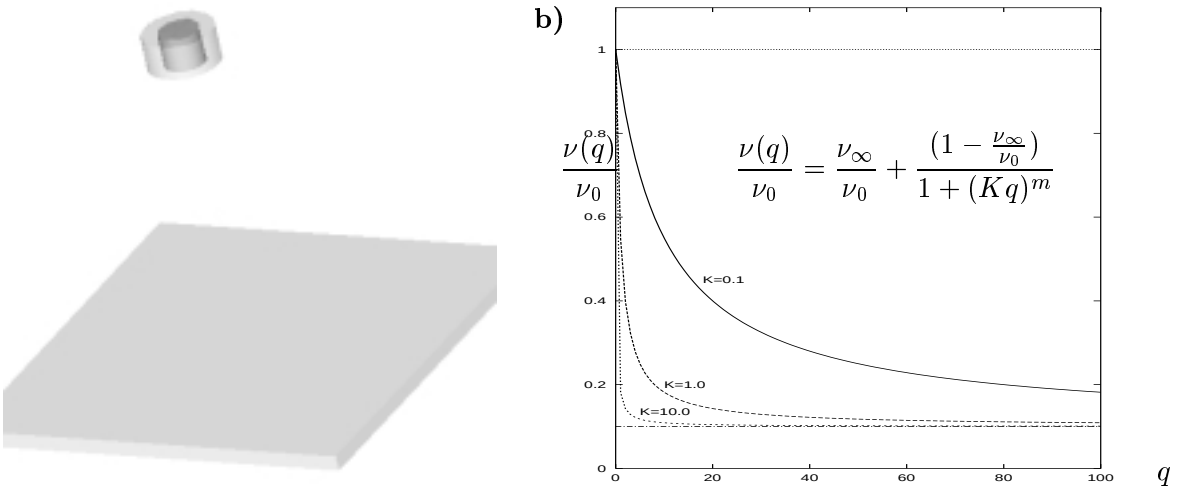

Figure 2. Problem specification and viscosity variation as a function of the parameter K.

5.1 Simulation of a jet impinging onto a flat surface

We consider a flat surface of dimensions 8cm $\times$ 8cm and an axisymmetric jet of 6mm diameter which is issuing from an axisymmetric nozzle into the flat surface at a prescribed velocity (see Fig. 2a). The following input data was employed: domain dimensions: 8 cm $\times$ 8 cm $\times$ 7 cm; mesh size: $80 \times 80 \times 70$ cells ($\delta x = \delta y = \delta z = 1$ mm); jet diameter (D): 8 mm; fluid velocity at the nozzle) (U): 0.25 ms^{-1} ; flat surface dimensions: 8 cm $\times 8$ cm with wall thickness 3 mm; nozzle dimensions: 8 mm diameter and 7 mm height; height of nozzle (H): 6 cm (distance of the nozzle to the flat surface); convergence criteria for the Poisson equation: EPS = 10^{-7} ; gravity was taken to act in the $z-$direction with $g_z = -9.81$ ms^{-2}. The fluid was modelled by the Cross model using $\nu_0 = 0.002$, $\nu_\infty = 0.0002$ and $m = 1$. For the scaling parameters U, D and ν_0 were employed so that $\mathrm{Re} = UD/\nu_0$ = 1.0 and Fr = 0.8924. The no-slip condition was applied on the flat surface walls.

To demonstrate that the technique presented in this paper simulates non-Newtonian flow we present five simulations through which we can observe non-Newtonian behaviour of a fluid modelled by the Cross model. The problem studied is the jet flow described above with the same geometry and input data; only the data regarding the viscosity will be different. For the first run we used the Cross model with the constant K = 0, obtaining a Newtonian flow with viscosity $\nu = \nu_0$; for the next three runs we employed the Cross model with K = 0.1, 1 and $K = 10$, respectively. In the fifth run we performed a Newtonian flow with the viscosity $\nu = \nu_\infty$ ($K \approx \infty$ in the Cross model). In these runs the scaling parameters were the same for each run, namely the supplied values of U, D and ν_0. Figure 3 displays three-dimensional flow visualizations at different times for these runs where, in the first column, we have the results of the first run (Newtonian flow with $\nu = \nu_0$); the second column displays the Cross model

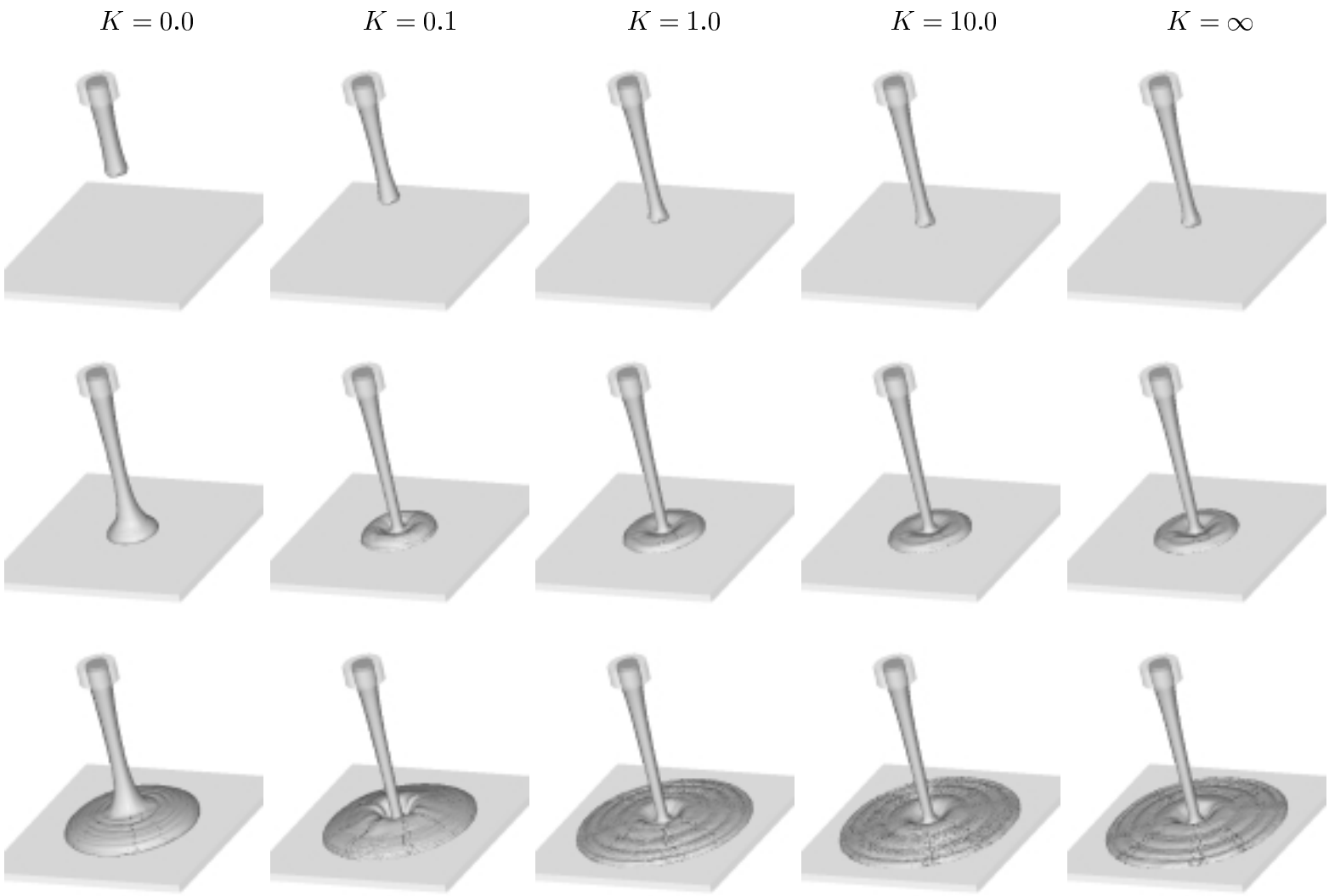

Figures 3. Numerical simulation of a non-Newtonian jet impinging onto a flat surface at times $t = 0.15$s (top row), 0.30s (middle row) and $t = 0.70$s (bottom row). Three-dimensional view.

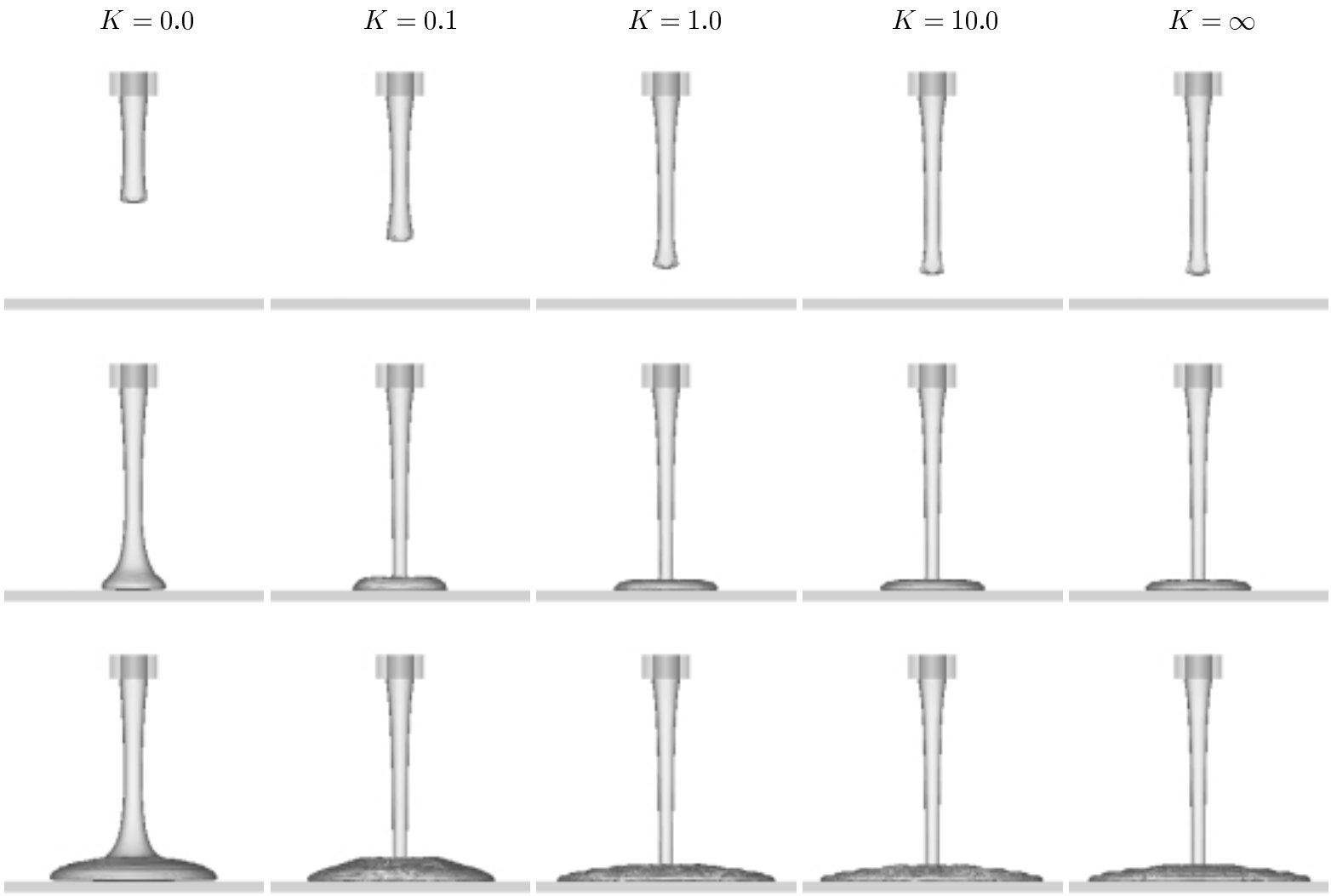

Figure 4. Numerical simulation of a non-Newtonian jet impinging onto a flat surface at times $t = 0.15$s (top row), 0.30s (middle row) and $t = 0.70$s (bottom row). Frontal view.

results with $K = 0.1$; third and fourth columns display the cross model results of $K = 1$ and $K = 10$, respectively. The last column displays the non-Newtonian results with $\nu = \nu_\infty$. The plots shown in Fig. 3 are taken at the same time frame. Figure 4 displays the front view visualization of these results. As we can observe in Figs. 3 and 4, the behaviour of the flow of a non-Newtonian fluid modelled by the Cross model is intermediate between the two Newtonian flows of $\nu = \nu_0$ and $\nu = \nu_\infty$. Indeed, as we can see in the Cross model (see Fig. 2b) the value of the constant K has a direct influence on the value of the viscosity and hence, the flow can approach the Newtonian flow with $\nu = \nu_0$ (if $K <<< 1$) or the Newtonian flow with $\nu = \nu_\infty$ (if $K >>> 1$) according to the value of K. As we can see from the plots, the larger the value of K the closer the flow is to Newtonian flow with $\nu = \nu_\infty$ (see Figs. 3 and 4, $K = \infty$). These results are consistent with the Cross model where for large values of K the value of viscosity approaches ν_∞ and therefore the flow should approach the Newtonian flow of $\nu = \nu_\infty$. Thus, the results shown in Figs. 3 and 4 give us confidence that they are correct.

Acknowledgements

We gratefully acknowledge support given by Fapesp and CNPq.

REFERENCES

E. Brasseur, M.M. Fyrillas, G.C. Georgiou and M. Crochet, The time-dependent extrudate-swell problem of an Oldroyd-B fluid with slip along the wall, *J. Rheol.*, **423**, 549-566 (1998).

D. Ding, P. Townsend and M.F. Webster, Computer modelling of transient flows of non-Newtonian fluids, *J. Non-Newtonian Fluid Mech.*, **47**, 339-356 (1993).

A. Castelo, M.F. Tomé, C.N.L. César, S. McKee, and J.A. Cuminato, Freeflow: An integrated simulation system for three-dimensional free surface flows, *Computing and Visualization in Science*, **2**, 199-210 (2000).

M. Griebel, T. Dornseifer and T. Neunhoeffer, Numerical Simulation in Fluid Dynamics: a practical introduction. SIAM publications (1997).

G. Mompean and M. Deville, Unsteady finite volume of Oldroyd-B fluid through a three-dimensional planar contraction, *J. Non-Newtonian Fluid Mech.*, **72**, 253-279 (1997).

M. Mäntylä, *An Introduction to Solid Modeling*, Computer Science Press (1988).

W. Shyy, H. S. Vdaykumar, M. M. Rao and R. W. Smith, Computational Fluid Dynamics with Moving Boundaries (Taylor and Francis, Washington, DC, 1996).

M.F. Tomé, A. Castelo, J.A. Cuminato and S. McKee, GENSMAC3D: A numerical method for solving three-dimensional free surface flows, paper under revision (2000).

M.F. Tomé, B. Duffy and S. McKee, A numerical technique for solving unsteady non-Newtonian free surface flows, *J. Non-Newtonian Fluid Mech.*, **62**, 9-34 (1996).

M.F. Tomé and S. McKee, GENSMAC: A computational marker-and-cell method for free surface flows in general domains, *J. Comput. Phys.*, **110**, 171-186 (1994).